

Continuous-time Quantum Monte Carlo Approach for Impurity Anderson Models with Phonon-assisted Hybridizations

Kazumasa HATTORI

Institute for Solid State Physics, University of Tokyo, 5-1-5, Kashiwanoha, Kashiwa Chiba 277-8581, Japan

We develop a continuous-time quantum Monte Carlo method based on a strong-coupling expansion for Anderson impurity models with phonon-assisted hybridizations for arbitrary number of phonon modes. As a benchmark, we investigate the two-channel Anderson model with a single phonon, and numerically demonstrate that an $SO(5)$ susceptibility composed of localized-electron charge and phonon-parity operators diverges logarithmically at non-Fermi liquid critical points in the model, which verifies the predictions by the boundary conformal field theory [K. Hattori: Phys. Rev. B **85** (2012) 214411].

KEYWORDS: multi-channel Kondo effects, continuous-time quantum Monte Carlo, non-Fermi liquid

1. Introduction

Kondo effects¹⁾ in electron-phonon coupled systems have been attracted great attention in recent years. Rare-earth based filled-skutterudites²⁾ and so-called 1-2-20 compounds³⁾ are candidates for various Kondo effects due to both magnetic and nonmagnetic origins. There, well-localized f-electrons are located at a “vibrating” ion inside a cage structure that provides conduction electrons to their Fermi surfaces. For long time, systems with strong electron-phonon interactions have been considered as those exhibiting various types of the Kondo effects.⁴⁾ Recently, magnetically robust heavy-fermion states in the filled-skutterudite $\text{SmOs}_4\text{Sb}_{12}$ ²⁾ have been attracted much attention due to the possible non-magnetic origin for the heavy fermion.^{5, 6)}

Apart from complexities in the f-electron orbital degrees of freedom in these compounds, a prototype model had been proposed already about thirty years ago by Yu and Anderson.⁷⁾ They analyzed a local atomic oscillation coupled with spinless two-channel conduction electrons. The atom is assumed to oscillate along one direction, say z-axis, and thus, an electron-phonon coupling induces hybridizations between conduction electrons with isotropic spherical wave and p_z -wave components. This is a so-called phonon-assisted hybridization process. Similar models have been analyzed in a line of discussions about possibility of two-channel Kondo effects in multi-level systems.^{8–13)}

Several authors extended the model proposed by Yu and Anderson to that includes the spin degrees of freedom and the Coulomb interaction U between localized electrons with the different spins and analyzed it by using the Wilson’s numerical renormalization group (NRG) method.^{14–17)} They found a line of non-Fermi liquid (NFL) fixed points characterized by spectra realized in the magnetic two-channel Kondo model⁴⁾ in the ground state phase diagram. Recently, on the basis of the boundary conformal field theory (BCFT), we investigated the

NFL and showed that the NFL in the weak-coupling regime is qualitatively different from that in the conventional magnetic two-channel Kondo model. We also showed that a crossover between the NFL of the magnetic two-channel Kondo model and the NFL in the weak-coupling regime, where $SO(5)$ fluctuations—combined local-electron charge and phonon parity fluctuations—are important, occurs, which can successfully explain the NRG results.¹⁸⁾

A main purpose of this paper is to develop a numerical tool applicable to electron-phonon systems with multi degrees of freedom, since, in systems with more than one or two phonon modes, the Hilbert space becomes too large to be handled by, for example, the NRG or the exact diagonalization. For the Holstein phonon coupled with an electron density, an efficient quantum Monte Carlo method was proposed.¹⁹⁾ However, the technique there is not applicable to the model with phonon-assisted hybridization. In this paper, we develop a continuous-time quantum Monte Carlo (CTQMC) method^{20–23)} to the Anderson impurity model with phonon-assisted hybridizations^{14, 15)} for multi phonon modes.

This paper is organized as follows. In Sect. 2, we will show a CTQMC algorithm for Anderson models with multi-channel conduction electrons and phonons. Benchmark tests in a small-size cluster problem will be shown to convince readers of the efficiency of the method. We will apply this to the model with one-dimensional phonons^{14, 15)} and discuss the criticality of the model in Sect. 3. Finally, Sect. 4 will summarize the present results and discuss possibilities of application of the present method to more complicated systems.

2. Continuous-time Quantum Monte Carlo Method

In this section, we will present our CTQMC algorithm for Anderson-type models with phonon-assisted hybridizations. For details of the basic algorithm for the impurity Anderson model, see the review paper.²³⁾ Af-

ter presenting models we use in Sect. 2.1, we will explain our algorithm of CTQMC in Sect. 2.2 and then show a benchmark result for a three-site cluster model in Sect. 2.3.

2.1 Model

We investigate an impurity Anderson model with phonon-assisted hybridization^{14,15)} generalized to one with M phonon modes,

$$H = H_c + H_l + H_{ph} + V + V^\dagger, \quad (1)$$

$$H_c = \sum_{\alpha=0}^M \sum_{\sigma} \int dk \epsilon_{k\alpha} c_{k\alpha\sigma}^\dagger c_{k\alpha\sigma}, \quad (2)$$

$$H_l = \sum_{\sigma} \epsilon_f f_{\sigma}^\dagger f_{\sigma} + U f_{\uparrow}^\dagger f_{\uparrow} f_{\downarrow}^\dagger f_{\downarrow}, \quad (3)$$

$$V = \sum_{\alpha=0}^M \sum_{\sigma} V_{\alpha\sigma}, \quad (4)$$

$$V_{\alpha\sigma} = \frac{v_{\alpha\sigma}}{\sqrt{M}} X_{\alpha} f_{\sigma}^\dagger \int dk c_{k\alpha\sigma}. \quad (5)$$

Here, the conduction electrons are written in the bases of spherical wave and $c_{k\alpha\sigma}$ indicates the conduction electron creation operator with the radial wavenumber k , the orbital $\alpha = 0, 1, \dots$, or M , and the spin $\sigma = \uparrow$ or \downarrow . f_{σ}^\dagger represents the localized electron creation operator with the spin σ and we assume it is isotropic s -orbital. ϵ_f and U are the localized electron energy level and the Coulomb interaction, respectively. $v_{\alpha\sigma}$ represents hybridization between localized and conduction electrons with α orbital and σ spin. $X_{\alpha} = X_{\alpha}^\dagger$ indicates phonon-displacement operators that are dimensionless quantities scaled by an appropriate length scale and have the same symmetry as the orbital α to make the Hamiltonian invariant. H_{ph} represents the Hamiltonian for phonons. In order to make computational cost small, we restrict ourselves to considering H_{ph} in which each X_{α} does not couple.²⁴⁾ For simplicity, throughout this paper, we will use a harmonic oscillator model for H_{ph} .

Hybridization processes without phonon assists are included in the V term with $\alpha = 0$ in eq. (5); $X_0 \equiv 1$. Corresponding to this, $c_{k0\sigma}^\dagger$ represents the creation operator of an s -orbital electron. When phonon oscillation amplitudes are small, X_{α} 's ($\alpha = 1, 2, \dots, M$) are, in the first-order approximation, represented by the linear-displacement operators x_{α} 's, which couple with p -wave components of conduction electrons $\int dk c_{k\alpha\sigma}$ with $\alpha = 1, 2, \dots, M$ around the impurity site in eq. (5). Here, in this case, M represents the dimensionality of the oscillation mode. One can also construct models that include processes with higher-order displacements such as $x_{\beta}x_{\gamma}$, $x_{\beta}x_{\gamma}x_{\delta}$, and so on, which couple with higher-order harmonics of spherical bases for conduction electrons.²⁵⁾ Although we do not discuss such models in this paper, our CTQMC method can handle these general hybridization processes.

2.2 Algorithm

In this subsection, we summarize the algorithm²⁶⁾ of the CTQMC applied to the model (1) on the basis of strong coupling expansion,^{21,23,27,28)} *i.e.*, perturbative expansions of V .

In terms of the infinite series of V and V^\dagger , the partition function Z for the model (1) is expressed as

$$Z = Z_c Z_l Z_{ph} \left\langle T_{\tau} \exp \left\{ - \int_0^{\beta} d\tau [V(\tau) + V^\dagger(\tau)] \right\} \right\rangle_0, \quad (6)$$

where T_{τ} represents time-ordered product and $\beta = 1/T$ with T being temperature. Z_c , Z_l and Z_{ph} are the partition function of non-interacting conduction electrons, that for localized electrons, and that for local phonons, respectively, and

$$\langle A \rangle_0 \equiv \frac{\text{Tr}\{A e^{-\beta(H_c + H_l + H_{ph})}\}}{Z_c Z_l Z_{ph}}. \quad (7)$$

As discussed by Werner *et al.*,²¹⁾ eq. (6) is evaluated by Monte Carlo simulations, in which the positions of $V(\tau)$ and $V^\dagger(\tau)$ along the imaginary time τ and also the perturbation order are sampled. In addition to the conduction- and the local-electron parts in Z , we need to calculate a part due to the phonons. For this, we need to evaluate

$$\langle T_{\tau} x_{\alpha}(\tau_1) x_{\alpha}(\tau_2) \cdots x_{\alpha}(\tau_{2k_{\alpha}}) \rangle_{ph}. \quad (8)$$

Here, $\langle A \rangle_{ph} \equiv \text{Tr}\{A e^{-\beta H_{ph}}\}/Z_{ph}$, and k_{α} is an integer with $2k_{\alpha}$ being the perturbation order of the α th phonon-assisted term, *i.e.*, the total number of vertices $v_{\alpha\uparrow}$ and $v_{\alpha\downarrow}$ in a configuration considered. Note that different α 's do not couple, since we have assumed that in H_{ph} each of the phonon mode is decoupled.

Unlike the case of Holstein phonons,¹⁹⁾ a simple canonical transformation does not work on absorbing the phonon terms into phase factors. This originates in the facts that the model is one with multiorbital in general and the off-diagonal hybridization density couples with the phonons, while there is the Coulomb interaction only for the f electrons, in contrast to the case in the Holstein-Hubbard model¹⁹⁾ where the density does in the electron-phonon coupling term. For actual calculations of eq. (8), we introduce a cutoff for the phonon Hilbert space for each α : N_{cut} . This part might not be a smart way, but it is at least efficient when one investigates models with multi-phonon modes and multi-orbital conduction electrons.

In practice, to make the computations fast, we store intermediate matrices in the matrix product calculations of eq. (8) and re-use them at later steps in the Monte Carlo simulations²⁸⁾ and also use the fast-update algorithm.²⁰⁾

For carrying out Monte Carlo samplings in the whole phase space of the partition function Z , we need to introduce appropriate update operations. In a single-impurity Anderson model, conventional updates are known to

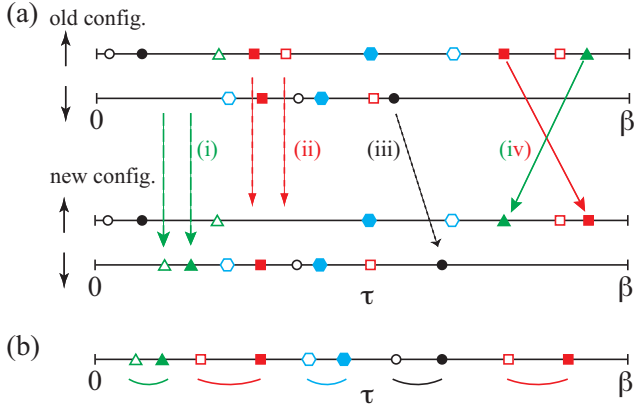


Fig. 1. (Color online) (a) Four update processes. The horizontal line represents imaginary time axis and the upper two represent “old” configuration with the spin \uparrow and \downarrow , and the lower two do “new” one. Open (filled) symbols represents $V_{\alpha\sigma}$ ($V_{\alpha\sigma}^\dagger$) and the types of symbols identify the orbital index α . Note that every open (filled) symbol is sandwiched by two filled (open) symbols and the total number of the open and the filled symbols are the same. (i) Inserting two vertices, (ii) removal of two vertices, (iii) shifting a vertex, and (iv) exchanging two vertices. (b) Typical vertex configuration without the exchange update.

be²¹⁾ (i) inserting two vertices $|v_{\alpha\sigma}|^2$, (ii) removing them, and (iii) shifting a vertex position in the imaginary time, as shown in Fig. 1 (a). A new update operation is necessary for realizing the random walk satisfying the Ergodicity in the present model in addition to conventional ones. That is (iv) exchanging two vertices $V_{\alpha\sigma}$ and $V_{\beta\sigma}$, or $V_{\alpha\sigma}^\dagger$ and $V_{\beta\sigma}^\dagger$ with $\alpha \neq \beta$, as depicted in Fig. 1 (a). Without this update, the vertex sequence along the imaginary-time axis is always paired in the same α , which is only a part of the whole phase space. See Fig. 1 (b). Upon the exchange update, only the conduction and phonon parts are affected, while the local-electron part is unchanged.

2.3 A benchmark

To check the algorithm explained in Sect. 2.2, in this subsection, we will show results for a finite-size system and compare the results by CTQMC with those by the exact diagonalization.

Here, we consider a harmonic-oscillator model for H_{ph} with $M = 1$ as an illustration of the efficiency of our method. We use a three-site model, which is equivalent to replacing the conduction electrons $c_{k0\sigma}$ by one electron c_σ and $c_{k1\sigma}$ by p_σ . Hamiltonian for this system is given as,

$$H_{3\text{sites}} = \sum_{\sigma} \left[(v_0 f_{\sigma}^\dagger c_{\sigma} + v_1 x f_{\sigma}^\dagger p_{\sigma} + \text{h.c.}) + \epsilon_f f_{\sigma}^\dagger f_{\sigma} \right] + U f_{\uparrow}^\dagger f_{\uparrow} f_{\downarrow}^\dagger f_{\downarrow} + \Omega \left(b^\dagger b + \frac{1}{2} \right), \quad (9)$$

where $x \equiv b^\dagger + b$ with b^\dagger being the phonon creation operator and Ω is the phonon energy. U is set to the energy unit $U = +1$, and we use $v_0/U = 0.2$, $v_1/U = 0.18$, $\epsilon_f/U = -0.5$, and $\Omega/U = 0.2$. In the following, we use the same N_{cut} both for the CTQMC and the exact

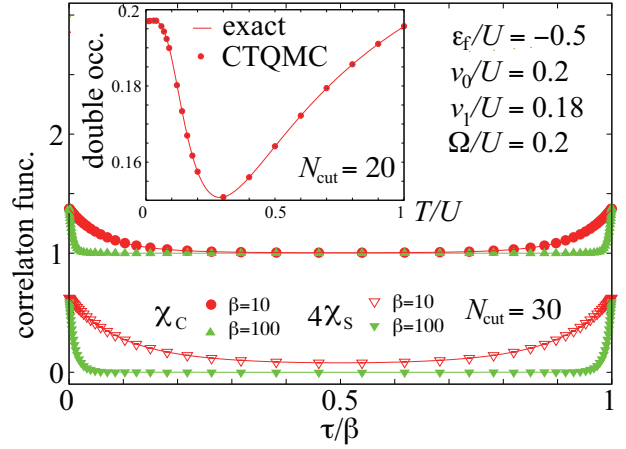


Fig. 2. (Color online) Imaginary time dependence of charge and spin susceptibilities for $\beta = 10$ and 100 . Symbols represent the CTQMC results and lines are those of the exact diagonalization. $N_{\text{cut}} = 30$ and $\epsilon_f/U = -0.5$, $v_0/U = 0.2$, $v_1/U = 0.18$, and $\Omega/U = 0.2$. Inset: temperature dependence of double occupancy for $N_{\text{cut}} = 20$ and the same parameters as in the main panel. Error bars are smaller than the symbol size.

diagonalization. Thus, the two results should be the same within the statistical errors in the CTQMC.

Figure 2 shows the imaginary time dependence of the charge susceptibility:

$$\chi_C(\tau) = \langle T_\tau [n_\uparrow(\tau) + n_\downarrow(\tau)] [n_\uparrow(0) + n_\downarrow(0)] \rangle, \quad (10)$$

and the spin susceptibility:

$$\chi_S(\tau) = \langle T_\tau [n_\uparrow(\tau) - n_\downarrow(\tau)] [n_\uparrow(0) - n_\downarrow(0)] \rangle / 4, \quad (11)$$

for $\beta = 10$ and 100 with $N_{\text{cut}} = 30$. Inset of Fig. 2 shows temperature dependence of double occupancy $\langle n_\uparrow n_\downarrow \rangle$ for $N_{\text{cut}} = 20$, where $n_\sigma = f_\sigma^\dagger f_\sigma$ and $\langle A \rangle$ represents the thermal average of operator A . The statistical errors for CTQMC data are smaller than the symbol sizes. One can clearly see that the CTQMC data reproduce the exact diagonalization ones within the statistical errors, which confirms the efficiency of our method.

3. Analysis of $M = 1$ Harmonic Model

In this section, we will show numerical results of the model with $M = 1$ and $H_{ph} = \Omega(b^\dagger b + 1/2)$ as in eq. (9) and we use spin-independent hybridizations in eq. (5): $v_{0\sigma} = v_0$ and $v_{1\sigma} = v_1$ as in Sect. 2.3. We use $\epsilon_{k\alpha} = v_F(k - k_F)$ with $v_F(k_F)$ being the Fermi velocity (wavenumber) for all α . Band width $2D$ is set to $D \equiv v_F \Lambda$, where Λ is the cutoff for the wavenumber and the density of states are set to a constant $1/(2D)$ from $-D$ to D by choosing appropriate values of v_F and Λ . Throughout this section, the cutoff of the phonon Hilbert space is set to $N_{\text{cut}} = 20$.

In previous studies of this model, a line of two-channel Kondo like NFL fixed points is found for $U \neq 0$.^{15,16)} Based on the NRG and the BCFT,¹⁸⁾ the NFL for small- U region turns out to be qualitatively different from that in the magnetic two-channel Kondo model. In particular, $\text{SO}(5)$ symmetric operators were identified and it was

predicted that susceptibilities of five-dimensional vector operators in the SO(5) sector diverge logarithmically at low temperatures. In the following, we concentrate on examining the divergence of the susceptibilities at the critical points of this model.

3.1 Susceptibilities

For the discussions in Sect. 3.2, we introduce following three susceptibilities, which are expected to show singular temperature dependence at the critical points.

First, we define a spin susceptibility given by

$$\chi_s^z(T) = \int_0^\beta d\tau \chi_s(\tau), \quad (12)$$

where $\chi_s(\tau)$ is given by eq. (11). The second is a coupled localized-electron's charge and phonon-parity susceptibility, which corresponds to an SO(5) vector susceptibility¹⁸⁾ with slight (not essential) simplifications,

$$\chi_{\mathcal{P}p}^z(T) = \int_0^\beta d\tau \left[\langle T_\tau \mathcal{P}(\tau) p_z(\tau) \mathcal{P}(0) p_z(0) \rangle - \langle \mathcal{P}(0) p_z(0) \rangle^2 \right], \quad (13)$$

$$p_z \equiv \sum_{n=0}^{N_{\text{cut}}} (-1)^n |n\rangle \langle n|, \quad (14)$$

$$\mathcal{P} \equiv (n_f - 1)^2, \quad (15)$$

where n represents the phonon number and $n_f = \sum_\sigma f_\sigma^\dagger f_\sigma$. Note that \mathcal{P} is the projection operator on $n_f = 0$ and 2 subspaces. The third one is a parity fluctuation of the phonons written as

$$\chi_p^z(T) = \int_0^\beta d\tau \left[\langle T_\tau p_z(\tau) p_z(0) \rangle - \langle p_z(0) \rangle^2 \right]. \quad (16)$$

According to the BCFT,¹⁸⁾ $\chi_s^z(T)$ and $\chi_{\mathcal{P}p}^z(T)$ diverge logarithmically $\sim -\ln T$ at the critical points of this model. It has been demonstrated that the diverging parts in $\chi_p^z(T)$ arise from $\chi_{\mathcal{P}p}^z(T)$ and the important parts for the divergence originate in the coupled localized-electron charge sectors with $n_f - 1 = \pm 1$ and the parity fluctuations.

3.2 Numerical results

Before discussing numerical results, we first comment about some technical aspects. First, we have found no noticeable negative sign problem in our line of calculations in this paper as in the calculations for the Anderson model.¹⁹⁾ Secondly, we have checked that the cut-off $N_{\text{cut}} = 20$ is sufficiently large for all temperature range we have examined. This can be checked by calculating probability distribution of phonon number n in the CTQMC; the probability for $n = N_{\text{cut}}$ is zero throughout the CTQMC sampling.

Now, let us start to discuss the results for small U regime, $U/D = 0.6$. Figure 3 shows temperature dependence of the susceptibilities $\chi_s^z(T)$ and $\chi_{\mathcal{P}p}^z(T)$. The spin

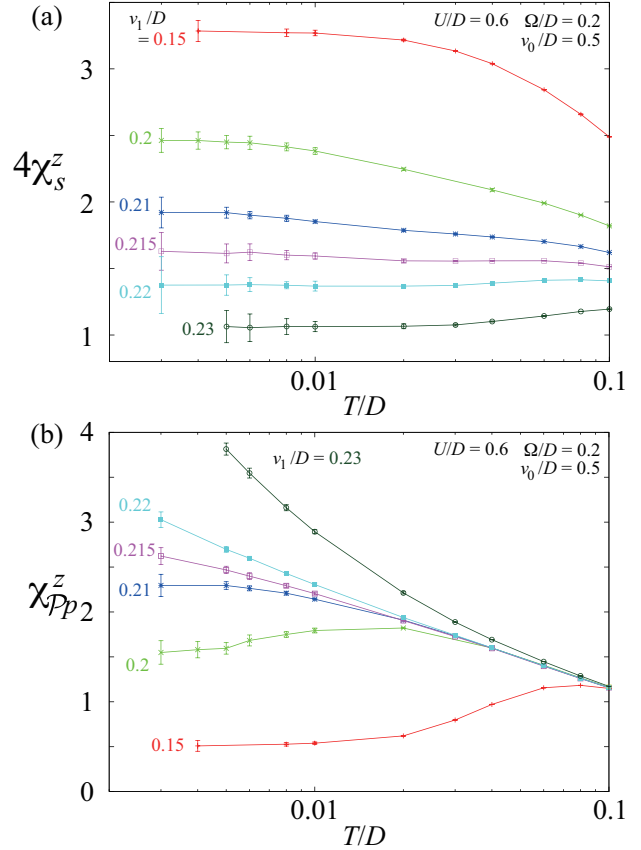


Fig. 3. (Color online) Temperature dependence of (a) $\chi_s^z(T)$ and (b) $\chi_{\mathcal{P}p}^z(T)$ for several values of v_1 's, $U/D = 0.6$, $v_0/D = 0.5$, and $\Omega/D = 0.2$ with $N_c = 20$.

susceptibility $\chi_s^z(T)$ [Fig. 3 (a)] shows no noticeable temperature dependence at low temperatures, while $\chi_{\mathcal{P}p}^z(T)$ shows logarithmic divergence for $v_1/D = 0.22$ as shown in Fig. 3 (b). The logarithmic divergence is expected to appear at the critical point, and thus, the critical point is located near $v_1/D \sim 0.22$. For a putative logarithmic singularity in $\chi_s^z(T)$, we cannot find noticeable one. We consider that the absolute value of the singularity is so small that it cannot be detectable within the present error bars in this small $U/D = 0.6$.

For larger U , the spin susceptibility shows a logarithmic increase at the critical point. Figure 4 shows $\chi_s^z(T)$ and $\chi_{\mathcal{P}p}^z(T)$ as a function of T for $U/D = 1.5$. One can see that $\chi_s^z(T)$ [Fig. 4 (a)] and $\chi_{\mathcal{P}p}^z(T)$ [Fig. 4 (b)] show logarithmic increases near the critical point $v_1/D \sim 0.225$. See the zoom up for $\chi_s^z(T)$ for $v_1/D = 0.225$. This indicates that the singularity in the spin sector becomes more prominent for $U/D = 1.5$ than for the smaller $U/D = 0.6$ in Fig. 3. As for $\chi_{\mathcal{P}p}^z(T)$, the absolute value becomes smaller than that for $U/D = 0.6$. This is because the system approaches the local moment regime as U increases. This crossover is consistent with the results in the NRG and the discussion in the BCFT.¹⁸⁾

For both $U/D = 0.6$ and 1.5, strong increases in $\chi_{\mathcal{P}p}^z(T)$ for v_1 larger than the critical value are due to

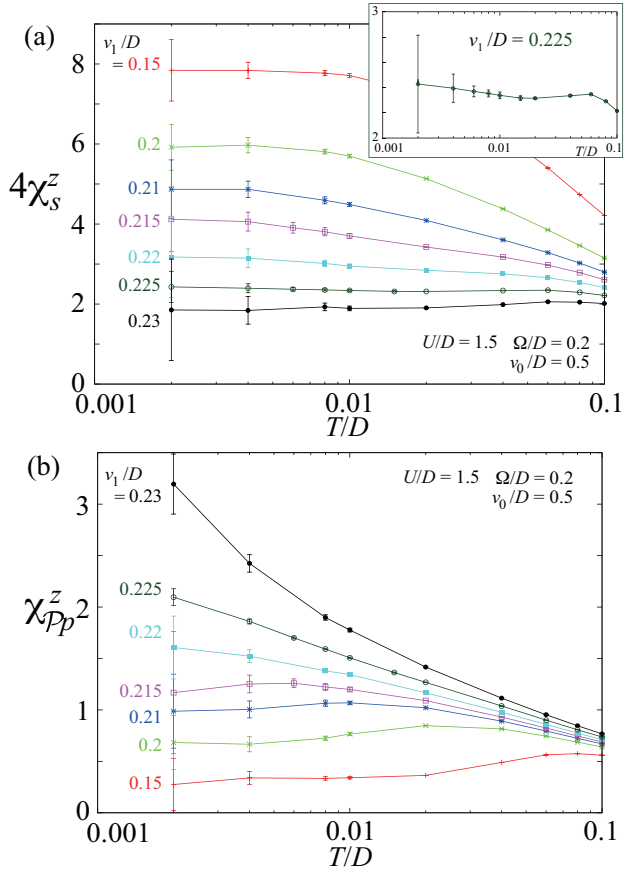


Fig. 4. (Color online) Temperature dependence of (a) $\chi_s^z(T)$ and (b) $\chi_{Pp}^z(T)$ for several values of v_1 's, $U/D = 1.5$, $v_0/D = 0.5$, and $\Omega/D = 0.2$ with $N_c = 20$. Inset in (a): zoom-up for $v_1/D = 0.225$.

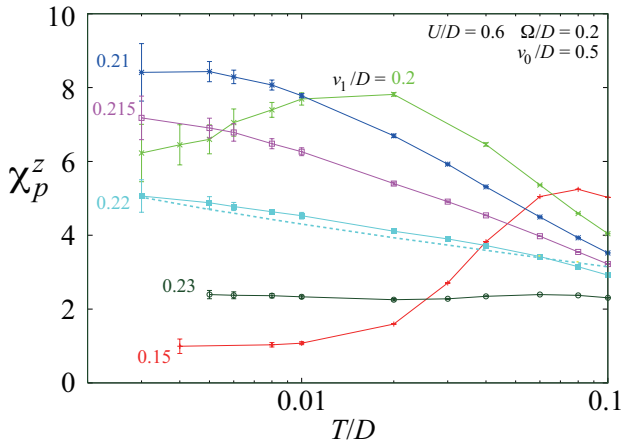


Fig. 5. (Color online) Temperature dependence of $\chi_p^z(T)$ for several values of v_1 's, $U/D = 0.6$, $v_0/D = 0.5$, and $\Omega/D = 0.2$ with $N_c = 20$. A dashed line represents $\chi_{Pp}^z(T) + 2$ for $v_1/D = 0.22$ from Fig. 3 (b).

the existence of nearly degenerate nonmagnetic states in the large v_1 limit, as discussed in the early work.¹⁶⁾ Thus, it is expected that they decrease for T smaller than the gap, but it is known that this is very small¹⁶⁾ and the CTQMC cannot reach such a small temperature.

We have also confirmed that the logarithmic temperature dependence in $\chi_p^z(T)$ near the critical point comes only from the subspace projected by \mathcal{P} . Figure 5 shows the temperature dependence of $\chi_p^z(T)$ for $U/D = 0.6$. For comparison, $\chi_{Pp}^z(T)$ near the critical point ($v_1/D = 0.22$) shifted by 2 is plotted by a dashed line. As seen in Fig. 5, both $\chi_p^z(T)$ and $\chi_{Pp}^z(T)$ show logarithmic increases for $v_1/D = 0.22$. Importantly, the logarithmic increase in $\chi_p^z(T)$ is quantitatively the same as those seen in $\chi_{Pp}^z(T)$ represented by the dashed line. Since $\chi_{Pp}^z(T)$ is a part projected by \mathcal{P} out of $\chi_p^z(T)$, this confirms that the singularity originates in the sector projected by \mathcal{P} , *i.e.*, $n_f = 0$ and 2 sectors, which is consistent with the prediction by the BCFT.¹⁸⁾

4. Discussions and Summary

We have developed a continuous-time quantum Monte Carlo method for impurity Anderson models with phonon-assisted hybridizations. The method can be applicable to models with several phonon modes and also non-harmonic phonon models within the restriction that each of phonon modes is decoupled. Even under this restriction, one can analyze various interesting models, such as a model with three-dimensional anharmonic potential $V(x, y, z) = \text{harmonic terms} + \eta_x x^4 + \eta_y y^4 + \eta_z z^4$ with η_i ($i = x, y, \text{ or } z$) being anharmonic parameters and one with an infinite-well potential as noted before.²⁴⁾ Advantage of using the CTQMC to solve models with multi phonon degrees of freedom is that one can treat its large Hilbert space in as small computational cost as in a single-phonon case (partly double for the exchange update).

An important point is that the computational cost decreases as the number of phonon modes *increases*, since, compared with the single-phonon case, the perturbation order for each mode $2k_\alpha$ in eq. (8) becomes smaller in multi-phonon cases. This is because the total perturbation order is not sensitive to the number of modes as discussed in the CTQMC for $SU(N)$ Coqblin-Schrieffer model.²⁹⁾ Thus, the perturbation order per orbital decreases, which leads to reduction of the number of the matrix products in eq. (8). This greatly reduces computational costs when the number of modes increases and opens possibilities for exploring various exotic Kondo effects in systems with multidegrees of freedom, which have never been reached by existing numerical (and also analytical) methods.

Additional Holstein phonons are easily handled by the canonical transformation as was done by Werner and Millis.¹⁹⁾ Extending the local electron part to one with orbital degrees of freedom is straight forward with slightly increasing computational costs and this is necessary extension for investigating more realistic systems. These are our future problems.

In the final part in Sect. 3, we have applied our CTQMC algorithm to the two-channel Anderson model with phonon-assisted hybridizations. The results have re-

vealed that fluctuations for the coupled electron-phonon degrees of freedom diverge logarithmically at low temperatures near the critical point. This is consistent with the previous theoretical analysis¹⁸⁾ and demonstrates the validity of the present method. As a next step, analyses of models with multi phonon modes are now in progress.

Acknowledgment

The author thanks H. Tsunetsugu and T. Sato for fruitful discussions. This work is supported by KAKENHI (Grant No. 30456199) and by a Grant-in-Aid for Scientific Research on Innovative Areas “Heavy Electrons” (Grant No. 23102707) of The Ministry of Education, Culture, Sports, Science, and Technology, Japan. A part of the numerical calculations was done at the Supercomputer Center at ISSP, University of Tokyo and also at Information Technology Center, University of Tokyo.

- 1) J. Kondo: Prog. Theor. Phys. **32** (1964) 37.
- 2) S. Sanada, Y. Aoki, H. Aoki, A. Tsuchiya, D. Kikuchi, H. Sugawara, and H. Sato: J. Phys. Soc. Jpn. **74** (2005) 246.
- 3) M. S. Torikachvili, S. Jia, E.D. Mun, S. T. Hannahs, R. C. Black, W. K. Neils, D. Martien, S. L. Bud’ko, and P. C. Canfield: Proc. Natl. Acad. Sci. U.S.A. **104** (2007) 9960.
- 4) D. L. Cox, and A. Zawadowski: Adv. Phys. **47** (1998) 599.
- 5) K. Hattori, Y. Hirayama, and K. Miyake: J. Phys. Soc. Jpn. **74** (2005) 3306.
- 6) T. Hotta: J. Phys. Soc. Jpn. **77** (2008) 103711.
- 7) C. Yu and P. W. Anderson: Phys. Rev. B **29** (1984) 6165.
- 8) K. Vladár and A. Zawadowski: Phys. Rev. B **28** (1983) 1564.
- 9) K. Vladár and A. Zawadowski: Phys. Rev. B **28** (1983) 1582.
- 10) K. Vladár and A. Zawadowski: Phys. Rev. B **28** (1983) 1596.
- 11) L. Moustakas and D. S. Fisher: Phys. Rev. B **51** (1995) 6908.
- 12) L. Moustakas and D. S. Fisher: Phys. Rev. B **55** (1997) 6832.
- 13) H. Kusunose and K. Miyake: J. Phys. Soc. Jpn. **65** (1996) 3032.
- 14) L. G. G. V. Dias da Silva and E. Dagotto: Phys. Rev. B **79** (2009) 155302.
- 15) S. Yashiki, S. Kirino, and K. Ueda: J. Phys. Soc. Jpn. **79** (2010) 093707.
- 16) S. Yashiki, S. Kirino, K. Hattori, and K. Ueda: J. Phys. Soc. Jpn. **80** (2011) 064701.
- 17) T. Hotta and K. Ueda: Phys. Rev. Lett. **108** (2012) 247214.
- 18) K. Hattori: Phys. Rev. B **85** (2012) 214411.
- 19) P. Werner and J. Millis: Phys. Rev. Lett. **99** (2007) 146404.
- 20) A. N. Rubtsov, V. V. Savkin, and A. I. Lichtenstein: Phys. Rev. B **72** (2005) 035122.
- 21) P. Werner, A. Comanac, L. de Medici, M. Troyer, and A. J. Millis: Phys. Rev. Lett. **97** (2006) 076405.
- 22) J. Otsuki, H. Kusunose, and Y. Kuramoto: J. Phys. Soc. Jpn. **78** (2009) 014702.
- 23) For a review of CTQMC, see E. Gull, A. J. Millis, A. I. Lichtenstein, A. N. Rubtsov, M. Troyer, and P. Werner: Rev. Mod. Phys. **83** (2011) 349.
- 24) This includes, *e.g.*, an infinite-well potential defined by $V(x, y, \dots) = 0$ for $|x| \leq a$, $|y| \leq b$, and \dots , while $V(x, y, \dots) = \infty$ for others, where $2a$, $2b$, \dots are the width of the well for x , y , \dots directions, respectively.
- 25) Of course, operators in a same irreducible representation can couple with each other. For example, isotropic combinations such as $\sum_{\beta} x_{\beta}^2$ couple to s -wave components of conduction electrons.
- 26) K. Hattori: 2011 ISSP Supercomputer Activity Rep., p. 23.
- 27) P. Werner and A. J. Millis: Phys. Rev. B **74** (2006) 155107.
- 28) K. Haule: Phys. Rev. B **75** (2007) 155113.
- 29) J. Otsuki, H. Kusunose, P. Werner, and Y. Kuramoto: J. Phys. Soc. Jpn. **76** (2007) 114707.